Squeezing Flow between Two Parallel Plates under the Effects of Maxwell Equation and Viscous Dissipation

Muhammad Bilal[1], Anwar Saeed[2,*], Ayesha Ali[3]

[1]Department of Mathematics, University of Peshawar, KP, Pakistan.
[2]Center of Excellence in Theoretical and Computational Science (TaCS-CoE), Faculty of Science, King Mongkut's University of Technology Thonburi (KMUTT), Thailand
[3]Department of Mathematics, Abdul Wali Khan University, Mardan, 23200, Khyber Pakhtunkhwa, Pakistan.
Corresponding author

Abstract

The unsteady, incompressible electroviscous fluid flow has been investigated with thermal energy transmission across two parallel plates. The upper plate is in motion, while the lower one is stationary. The flow is governed by the Navier-Stokes equations, which are combined with the Maxwell equation. The system of nonlinear PDEs is simplified to a system of ODEs along with their boundary conditions using Von-Karman's transformation. For the problem's analytic solution, the homotopy analysis method (HAM) has been used, and the result is compared to the Runge Kutta method of order four and latest computational technique parametric continuation method (PCM) to determine the validity of the scheme. It has been noted that the outcome is reflected with the best settlement. Interest physical constraints are graphically illustrated and briefly discussed in relation to velocity, temperature, magnetic strength profile, skin friction, and Nusselt numbers. The axial velocity of the fluid reduces by the action of Reynold numbers R_1. The magnetic profile intensity is reduced as the Batchelor number rises, while the magnetic strength is boosted as the magnetic Reynolds number R_3 increases.

Keywords: Variable magnetic field; Maxwell equation; Reynolds number; HAM; Batchelor number; RK4.

Nomenclature	
Greek Symbols	
α	Thermal diffusivity
β	Thermal expansion coefficient
B_0	Magnetic strength
η	Scaled boundary layer coordinate

Email addresses: bilalchd345@gmail.com (M. Bilal), anwar.sae@kmutt.ac.th (A. Saeed), ayeshaali666@yahoo.com (A. Ali)

μ	Dynamic viscosity
μ_2	Magnetic permeability
$v = \dfrac{\mu}{\rho}$	Kinematic viscosity
ρ	Density
K	thermal conductivity
ρ_{cp}	Heat capacity
σ	Fluid electric conductivity
μ_0	Free surface permeability
V	Fluid viscosity
T_0	constant temperature
$Pr = \dfrac{\rho_{cp}}{K}$	Prandtl number
$R_1 = \dfrac{H^2}{v}$	Reynold number
$R_2 = \dfrac{\alpha H^2}{2v}$	Reynold number based on flow speed
$R_3 = \dfrac{M_0}{R\sqrt{v\rho}}$	Magnetic Reynold number
$Bt = \sigma\mu_2 v$	Batchelor number

1. Introduction

The association of fluid flow with a magnetic effect is a well-known area of fluid dynamics, which is known as magnetohydrodynamics (MHD). Such flow is usually used in bearings, food production and cooling towers, electrical devices, chemical, and mechanical operations, fog forming and dispersion, and crop protection [1]. Stefan [2] was the first to look at squeezing flow for lubrication in a device. Mehmood *et al.* [3] investigated squeezed flow with energy transmission across an impermeable wall. Mustafa *et al.* [4] reported heat transition in a squeezed viscous flow across two plates. Squeezing conducting flow across pair of plates is scrutinized by Hauck et al. [5]. Bhatti *et al.* [6] used a Darcy medium for the simulation to investigate the heat distribution of conducting flow across a parallel channel. The comparison between DTM and numerical methods suggests that the DTM approach for solving nonlinear differential equations is very flexible and reliable. Ikram *et al.* [7] reported a fractional model for the free convective Brinkman form nanofluid that retained hybrid nanoparticles in place across bounded parallel plates. The impact of a magnetic force on water-based Fe_2O_3 and

CNTs nanoliquids across a circular sheet is simulated by Gul *et al.* [8]. MWCNTs have a larger effect on heat flow and velocity profile, according to the findings. Alhowaity *et al.* [9] used computational methods to

investigate the behavior of a hybrid nanofluid flow over a moving sheet. Bilal et al. [10] reported the characteristics of electroviscous trihybrid nanoliquid flow across compressing parallel infinite sheets. It was discovered that the charge transport rate increases when the Lewis number and activation energy are increases. Algehyne et al. [11] used PCM approach to study the hydromagnetic flow of a particular kind of water-based ferrofluid, which included motile microbes and nano particulates, through a permeable erect mobile substrate.

In both Newtonian and Non-Newtonian fluid flow problems, the MHD principle is crucial. MHD has a variety of uses and speeds, including flow meters, magnetic drug-controlled sensors, blood flow tests in astrophysics, nuclear reactors, and pumps, among others [12-15]. Helmy [16] involved a standard perturbation approach to finding the solution for convective MHD flow past over a plate. A three-dimensional solution of time-dependent hybrid nanoliquid flow with MHD and heat transport features induced by the upward/downward movement of a wavy disc has been investigated by Ahmadian et al. [17]. As compared to a flat surface, the wavy surface facilitates heat transfer by up to 15%. Rashidi *et al.* [18] calculated the MHD fluid flow in terms of bivariate function using the RK4 approach and the Shooting technique. By taking the Riga plate Lv *et al.* [19] described the nanoliquid flow in order to improve the heat transmits power for research and industrial applications. Tassaddiq *et al.* [20] Explored nanofluid flow over an infinite surface. To further analyze the fine point of nanofluid flow, they added the effect of the magnetic field. Sharma and Sood *et al.* [21] Addressed the consequences of double stratifications and magnetic fields on the convective flow of Jeffrey nanoliquid. Shuaib *et al.* [22] and Hayat *et al.* [23] documented the slip flow with convective heat transition and variable magnetic impact. The discoveries show that the MHD has a momentous impact on the fluid flow's velocity and energy transmission. Khashi'ie et al. [24] investigated the thermal properties and flow behavior of a Cu-Al2O3/water nanoliquid in a 2D system with a moving plate using MHD unsteady isolated stagnation point flow. Ali et al. [25] reported the effects of energy transference on the movement of a Jeffery nanofluid with submerged nanomaterials in the context of an applied magnetics flux across a nonlinear stretchy surface, under the upshots of Brownian and thermal radiation.

Viscous dissipation has huge beneficial uses in different fields such as in fluid mechanics, medicine, engineering, electrochemistry, and biological physics. The heat transmission together with the dissipation of viscosity has received significant attention from researchers [26-28]. A comprehensive note regarding the impact of viscous dissipation on a fluid flow is firstly presented by Gehart *et al.* [29] in 1969. The authors used the technique of perturbation to gain the solution of governing equations. Ndolene [30] investigated Stokes's 1st together with the consequences of dissipation. For exact expressions of velocity and temperature profile, he applied the mathematical tools of the Laplace and Fourier transform techniques. Numerical examination of the hybrid nanofluid flow over a slender stretching surface discussed in [31]. The authors assumed the viscous dissipation in their accounts. He used relative similarity variables to make their governing PDEs to the ordinary differential equations. They highlighted in their conclusion that a larger Eckert number rise the temperature field. Despite all the mentioned significances, the term viscous dissipation is ignored by many researchers during their research work [32, 33]. Keeping in view the importance of viscous dissipation, we considered viscous dissipation flow together with the influence of the Maxwell equation.

For the solution of PDEs and ODEs, two analytical methods (Asymptotic and Perturbation) were traditionally used. Which are commonly used in finance, engineering, and science for the analytic solution of various problems, but both asymptotic and perturbation techniques are based on large/small parameters. Which are only true for nonlinear equations with weak coefficients. In 1992, Liao [34] published a technique for analytical approximation, called the Homotopy Analysis approach, which is very useful for the solution of nonlinear PDEs, because it does not rely on large/small parameters. Liao [35] has explained the HAM strategy for solving

nonlinear ODEs. Bilal *et al.* [36] used the Homotopy analysis approach to analyze the Darcy convective flow of the nanoliquid into an inclined expanding cylinder. Gul *et al.* [37] evaluated the energy propagation inside the space between disc and cone across hybrid nanoliquid. They investigated four separate cases of flow between cone and disc using the HAM technique. Gul *et al.* [38] analyzed the fluid flow over a horizontally traveling thin needle using the HAM approach. The thermal dynamics and fluid velocity are thought to be highly influenced by the needle's composition, including its size and form.

In the field of hydrodynamics, the magnetic force has numerous uses, particularly in the electrically conductive fluid. There are several applications for compressing flow between two plates. We expand the concept of Rehan *et al.* [39] in light of the uses of conducting squeezed flow that have already been outlined in the preceding paragraphs. They looked into incompressible fluid flow across a rotating disc in a steady state. The squeezing flow of viscous fluid with heat transition under magnetic effects has been investigated using the known mathematical model. The next part contains the problem's formulation and discussion.
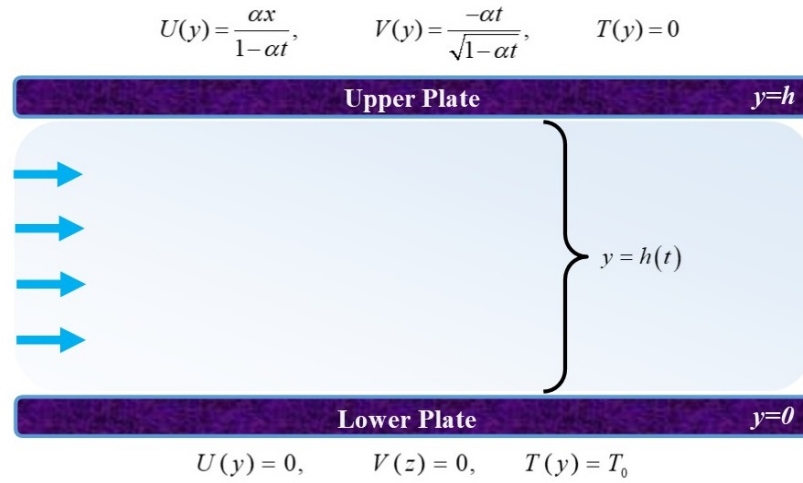
Figure 1: Fluid flow between two plates.

2. Mathematical Formulation

We considered the fully developed, axisymmetric, pressure-driven time-dependent flow in a cartesian coordinate system across two plates. With velocity $U=0$, the lower plate is at rest, while $U(h) = U_w$ is the stretching velocity of the upper plate. The gap between the plates is h. Figure 1 depicts the flow geometry. Both x-axis and y-axis are subjected to a variable magnetic field B_0. Temperature T_0 is maintained on the lower layer and upper plate T_∞

The Lorentz force $\vec{J} \times \vec{B}$ is applied to the equations for nonconducting plates. The continuity equation, energy, and Maxwell equation, as well as their boundary conditions, are modeled as follows [39, 40]:

$$U_x + V_y = 0 \tag{1}$$

$$U_t + UU_x + VU_Y = P_x + \upsilon\left(U_{xx} + U_{yy}\right) + \frac{1}{\rho\mu_2}\left(ByBx_y + ByBy_x\right) \tag{2}$$

$$V_t + UV_x + VV_Y = P_y + \upsilon\left(V_{xx} + V_{yy}\right) + \frac{1}{\rho\mu_2}\left(BxBy_x + BxBx_y\right) \tag{3}$$

$$T_t + UT_x + VT_y = \frac{K}{\rho C_p}\left(T_{xx} + T_{yy}\right) \tag{4}$$

$$Bx_t = UBy_y + ByU_y - VBx_y + BxV_y + \frac{1}{\rho\mu_2}(Bx_{xx} + Bx_{yy}) \tag{5}$$

$$By_t = -UBy_x - ByU_x + VBx_x + BxV_x + \frac{1}{\rho\mu_2}(By_{xx} + By_{yy}) \tag{6}$$

The boundary conditions are:

$$U(y) = 0, \ V(z) = 0, \ T(y) = T_0, \ Bx(y) = 0, \ By(y) = \frac{M_0}{(1-\alpha t)} \ \text{at} \ y = 0, \tag{7}$$

$$U(y) = \frac{\alpha x}{1-\alpha t}, \ V(y) = \frac{-\alpha t}{\sqrt{1-\alpha t}}, \ T(y) = 0, \ Bx = 0, \ By(y) = \frac{M_0}{1-\alpha t} \ \text{at} \ y = h$$

Here, K, μ_2, ρ illustrate the thermal diffusion ratio, magnetic permeability, and density respectively, while u and v are the velocity component.

The following mechanism has been used to convert the PDE scheme into an ODE system [40]:

$$\left. \begin{array}{l} u = \dfrac{\alpha x}{(1-\alpha t)} f'(\eta), \quad v = \dfrac{-\alpha H}{\sqrt{(1-\alpha t)}} f(\eta), \quad \theta(\eta) = \dfrac{T - T_\infty}{T_0 - T_\infty}, \quad Bx = \dfrac{\alpha x M_0}{2H(1-\alpha t)} m'(\eta), \\[4mm] By = \dfrac{M_0}{\sqrt{(1-\alpha t)}} h(\eta), \quad \eta = \dfrac{y}{H(1-\alpha t)^{\frac{1}{2}}}. \end{array} \right\} \tag{8}$$

Using Eq. (8) in Eqs. (1)-(4), the following ODE scheme is formed (7):

$$f'''(\zeta) = R_1\zeta f''(\zeta) + 2R_1 f''(\zeta) + 3R_1 f'(\zeta)f''(\zeta) + R_1 f(\zeta)f'''(\zeta) - \frac{R_3 R_1}{2} m'(\zeta)m''(\zeta) \tag{9}$$

$$- \frac{R_3 R_1}{2} h(\zeta)m''(\zeta) + \frac{R_3 R_1}{2} m'(\zeta)h'(\zeta),$$

$$\theta''(\zeta) = Pr R_2 \zeta \theta'(\zeta) - 2Pr R_2 f(\zeta)\theta'(\zeta), \tag{10}$$

$$m'''(\zeta) = \frac{2R_2}{R_1}\zeta Btm''(\zeta) + \frac{4R_2}{R_1^2} Btm'(\zeta) - \frac{2Bt}{R_1} f'(\zeta)h'(\zeta) - 2\frac{Bt}{R_1} f''(\zeta)h(\zeta) \tag{11}$$

$$- \frac{4R_2 Bt}{R_1} f'(\zeta)m''(\zeta) - \frac{2R_2^2 Bt}{R_1} f'(\zeta)m'(\zeta),$$

$$h''(\zeta) = R_2 Bth'(\zeta)\zeta + R_2 Bth(\zeta) + 2R_2 Bth(\zeta)f'(\zeta) + \frac{2R_2^2 Bt}{R_1} f(\zeta)m'(\zeta). \tag{12}$$

The transformed conditions are:

$$\left. \begin{array}{l} f(0) = 0, \ f'(0) = 0, \ \theta(0) = 1, \ m'(0) = 0, \ h(0) = 1, \\[2mm] f(1) = 1, \ f'(1) = 1, \ \theta(1) = 0, \ m'(1) = 0, \ h(1) = 0 \end{array} \right\} \tag{13}$$

3.   HAM Solution

To solve equations (9)-(12) and (13), the Homotopy Analysis Method has been employed. Liao is the one that presented HAM [34, 35].

The initial guesses for velocity, temperature and magnetic fields are:

$$f_0(\zeta) = -r\zeta(\zeta^2 - 2\zeta +)',$$

$$\theta_0(\zeta) = -\zeta + 1,$$

$$m_0(\zeta) = \frac{\zeta}{2},$$

$$\theta_0(\zeta) = \zeta.$$

(28)

The linear operators λ_f, λ_θ, λ_m, and λ_h, are expressed as

$$\Pi_f = \frac{d^4 f}{d\zeta^4}, \quad \Pi_\theta = \frac{d^2 \theta}{d\zeta^2}, \quad \Pi_m = \frac{d^3 m}{d\zeta^3}, \quad \Pi_h = \frac{d^2 h}{d\zeta^2}.$$

(29)

The expend form of the Π_f, Π_θ, Π_m, Π_h, are obtained by Taylor's Series expansion

$$\Pi_f(\xi_1 + \xi_2\zeta + \xi_3\zeta^2 + \xi_4\zeta^3), \quad \Pi_\theta(\xi_5 + \xi_6\zeta),$$

$$\Pi_m(\xi_7 + \xi_8\zeta + \xi_9\zeta^2), \quad \Pi_h(\xi_{10} + \xi_{11}\zeta),$$

(30)

$$f(\zeta,\ell) = f_0(\zeta) + \sum_{x=1}^{\infty} f_x(\zeta)\ell^x,$$

$$\theta(\zeta,\ell) = \theta_0(\zeta) + \sum_{x=1}^{\infty} \theta_x(\zeta)\ell^x,$$

$$m(\zeta,\ell) = m_0(\zeta) + \sum_{x=1}^{\infty} m_x(\zeta)\ell^x,$$

$$h(\zeta,\ell) = h_0(\zeta) + \sum_{x=1}^{\infty} h_x(\zeta)\ell^x,$$

(31)

Now

$$f_x(\zeta) = \frac{1}{x!}\frac{\partial f(\zeta;\ell)}{\partial \zeta}\bigg|\ell = 0,$$

$$\theta_x(\zeta) = \frac{1}{x!}\frac{\partial \theta(\zeta;\ell)}{\partial \zeta}\bigg|\ell = 0,$$

$$m_x(\zeta) = \frac{1}{x!}\frac{\partial m(\zeta;\ell)}{\partial \zeta}\bigg|\ell = 0,$$

$$h_x(\zeta) = \frac{1}{x!}\frac{\partial h(\zeta;\ell)}{\partial \zeta}\bigg|\ell = 0,$$

(32)

The system can be written as

$$L_f\left|f_x(\zeta) - N_x f_{x-1}(\zeta)\right| = \Pi_f R_x f(\zeta),$$

$$L_\theta\left|\theta_x(\zeta) - N_x\theta_{x-1}(\zeta)\right| = \Pi_\theta R_x\theta(\zeta),$$

$$L_m\left|m_x(\zeta) - N_x m_{x-1}(\zeta)\right| = \Pi_m R_x m(\zeta),$$

$$L_h\left|h_x(\zeta) - N_x h_{x-1}(\zeta)\right| = \Pi_f R_x h(\zeta),$$

(33)

4.   Error Analysis

We performed the first error analysis to define the problem to ensure that our results are accurate up to the lowest residual error scale. Until evaluating and providing physical forecasts, we analyze an error to determine the accuracy of the proposed method. For this purpose, Tables [1, 2] and Figure 2 are drawn.
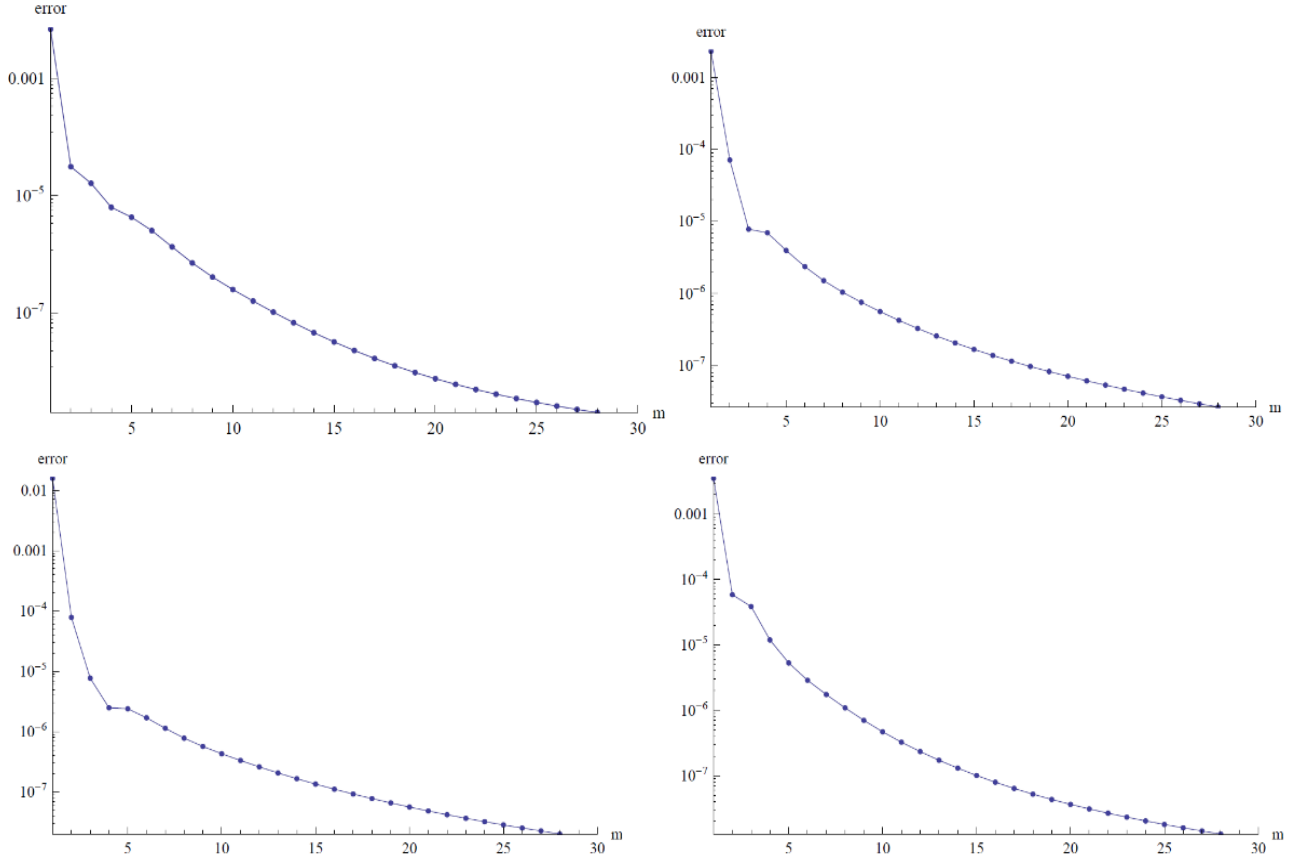
Figure 2: Residual error for velocity, magnetic strength and thermal energy profile.

Table 1: Optimal convergence for the different order of approximation.

Order of approximation	h_f	h_θ	h_h	h_m	ε_m^t
0	0	0	0	0	$1.20563 \, x10^0$
1	-0.600601	-0.4	-0.882872	-0.5	$3.96396 \, x10^{-3}$
2	-0.849895	-0.283307	-0.724752	-0.286707	$2.41117 \, x10^{-5}$
3	-0.45879	-0.509151	-0.140321	-0.219345	$4.95754 \, x10^{-4}$
4	-0.358388	-0.172129	-0.652075	-0.174164	$5.02034 \, x10^{-5}$

Table 2: Individual averaged squared residual errors.

M	ε_m^f	ε_m^θ	ε_m^h	ε_m^m
1	2.9843×10^{-3}	9.76043×10^{-3}	5.33289×10^{-4}	1.86872×10^{-6}
3	4.09773×10^{-5}	6.7172×10^{-5}	9.57857×10^{-6}	6.28919×10^{-5}
5	$5.92848 \times10-6$	1.20581×10^{-6}	4.66723×10^{-6}	9.28047×10^{-6}
7	2.19039×10^{-6}	1.53567×10^{-7}	1.92271×10^{-6}	2.72748×10^{-6}
9	7.54318×10^{-7}	4.51081×10^{-8}	9.29069×10^{-7}	1.11728×10^{-6}
11	2.9164×10^{-7}	1.82423×10^{-8}	5.17961×10^{-7}	5.23161×10^{-7}

13	1.28146×10^{-7}	8.80226×10^{-9}	3.13431×10^{-7}	2.74055×10^{-7}
15	6.1026×10^{-8}	4.83813×10^{-9}	2.02176×10^{-7}	1.5801×10^{-7}
17	3.14437×10^{-8}	2.94572×10^{-9}	1.3766×10^{-7}	9.8419×10^{-8}
19	1.75654×10^{-8}	1.93471×10^{-9}	9.79619×10^{-8}	6.54089×10^{-8}
21	1.06001×10^{-8}	1.34245×10^{-9}	7.22891×10^{-8}	4.59022×10^{-8}
23	6.87338×10^{-9}	9.69208×10^{-10}	5.49757×10^{-8}	3.36943×10^{-8}
25	4.75238×10^{-9}	7.19818×10^{-10}	4.28704×10^{-8}	2.56594×10^{-8}
27	3.47101×10^{-9}	5.4693×10^{-10}	3.40887×10^{-8}	2.01325×10^{-8}
29	2.65187×10^{-9}	4.14909×10^{-10}	2.75144×10^{-8}	1.618×10^{-8}
30	2.35209×10^{-9}	3.48062×10^{-10}	2.49138×10^{-8}	1.46085×10^{-8}

Table 1 represents the parameters (h_f, h_θ, h_h, h_m,) optimal convergence for the different order of approximation. Table 2 revealed the Individual averaged squared residual errors. From, Figure 2 it can be shown that as the order of approximation for different physical parameter values rises, the total average square errors and average square residual errors decrease.

5.   Analysis and Discussion

By using HAM, the system of nonlinear Eqs. (9-12) and the boundary state Eq. (13) has been solved. The Runge Kutta of order four procedures is used to validate the numerical results. The flow dynamics are revealed in Figure 1.

Figure 3(a) shows the effects of Reynolds number R_1 on velocity in the axial direction $f(\xi)$. The increment in Reynolds number reduces the kinematic viscosity of the fluid, which causes the inclination of the axial velocity. Fig. 3(b) elaborates the upshots of the magnetic Reynolds number versus the axial velocity $f(\xi)$. It can be perceived that dormancy of R_3 reduces the induction influence on fluid flow, as a result, the axial velocity increase.

Fig. 3(c) reveals that the radial velocity of a fluid increases as the Reynolds number raises, but at 0.5, the fluid velocity started to decline, and the radial velocity $f'(\xi)$ steadily decreases as the Reynolds number intensifies.

Fig. 3(d) depicts the influence of the magnetic Reynolds number R_3 on radial velocity $f'(\xi)$. The impact of magnetic Reynold number R_3 reduces the radial velocity of the fluid. But, at $\eta = 0.3$ the flow exhibits inverse behavior and started inclination. The B_0 field is perpendicular to the radial velocity $f'(\xi)$ because as the magnetic effect reduces, the fluid flow tends to increase.

$R_1 = 0.1, 0.2, 0.3, 0.4.$

$R_3 = 0.2, 0.4, 0.6, 0.8.$

(a)

(c)   **(d)**
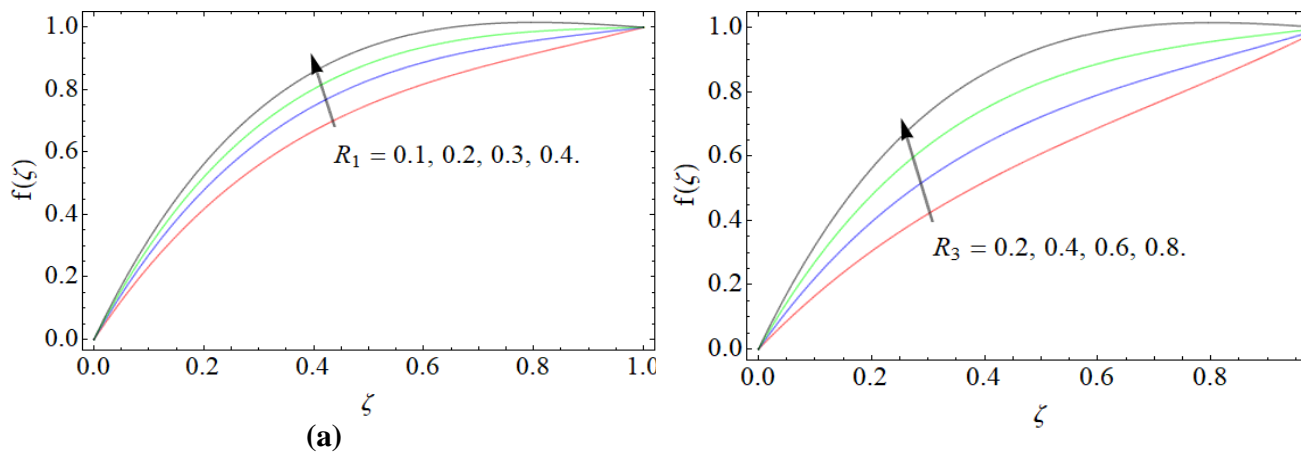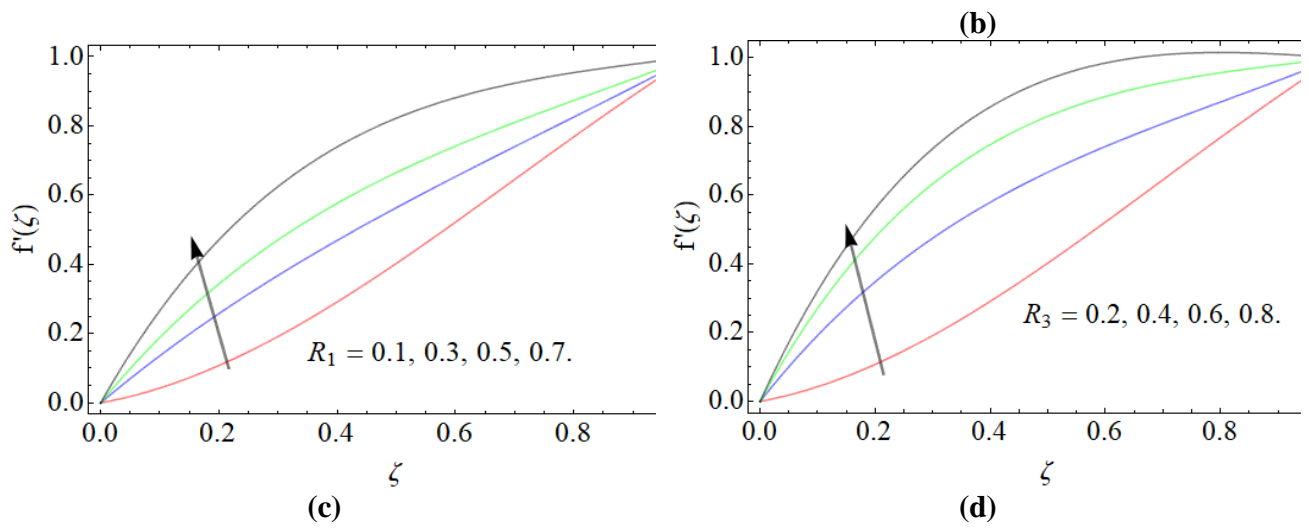
Figure 3: Axial and velocity outlines versus (a) & (c) Reynolds number R_1 (b) & (d) Magnetic Reynolds number R_3.

Figure 4(a) categorizes the significances of Prandtl number Pr on the energy profile $\theta(\xi)$. Physically, the fluid with high Prandtl effects has the less thermal capability. That's why the fluid temperature dropped with the action of the Prandtl effect. Fig. 4(b) describes the possessions of the Reynolds number on the thermal energy transition $\theta(\xi)$. When the Reynolds number rises, the fluid's kinematic viscosity decreases, increasing the fluid's kinematic capacity. The fluid temperature raised as a result of the high kinematics capacity.

(a)   **(b)**
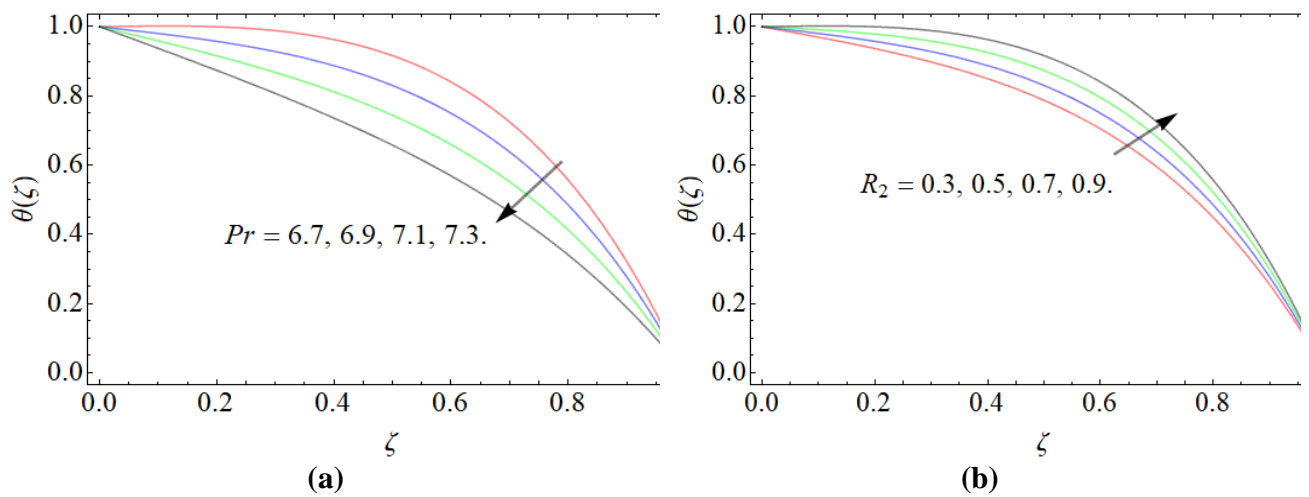
Figure 4: Energy outlines versus (a) Prandtl number Pr (b) velocity Reynolds number R_2.

Figure 5(a) represents the upshots of the Batchelor number on the magnetic power profile $m'(\xi)$. The magnetic permeability of fluid enhances as Bt grows. That's why magnetic strength profile show reduction with the positive increment of Batchelor number. Similarly, as the Reynolds number R_2 raises, the magnetic resistance of the fluid rises, which is shown in Fig. 5(b).
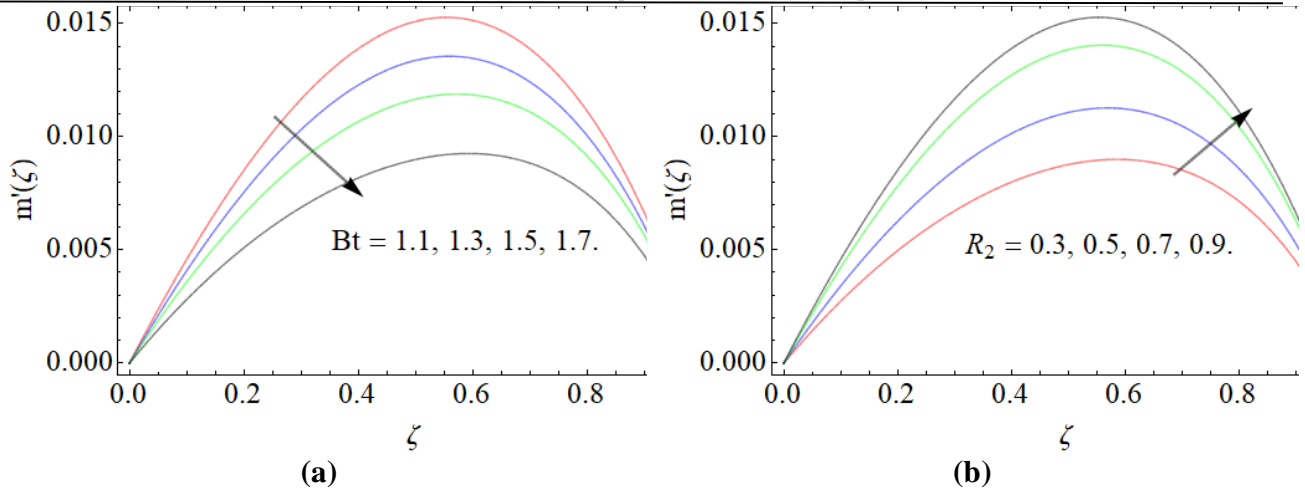
Figure 5: Axial magnetic strength profile versus (a) Batchelor number Bt (b) velocity-based Reynolds number R_2.

The effects of *Bt* and R_2 on the magnetic strength profile are presented in Fig. 6(a) & 6(b). As the parameter *Bt* reduces, the magnetic strength on fluid decreases, but the magnetic strength on fluid flow often decreases with cumulative effects of R_2. In Fig. 7, the convergence of the HAM technique is evaluated, and convergence zones of velocities and energy profiles are reviewed. The quantitative analysis between skin friction and Nusselt number for physical parameters *Pr* and *Bt* are illustrated through Tables 3 & 4 respectively. From table 4, it can be concluded that the present results are in best settlement with the published work. Table 5 displays the comparative analysis between HAM and RK4 methods.
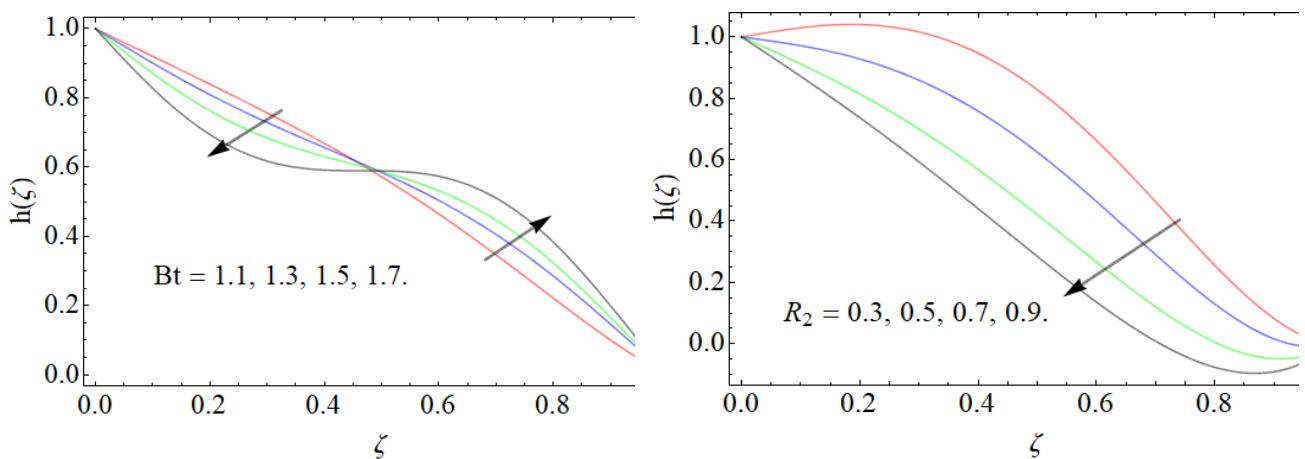
Figure 6: Radial magnetic strength profile versus (a) Batchelor number *Bt* (b) velocity Reynolds number R_2.
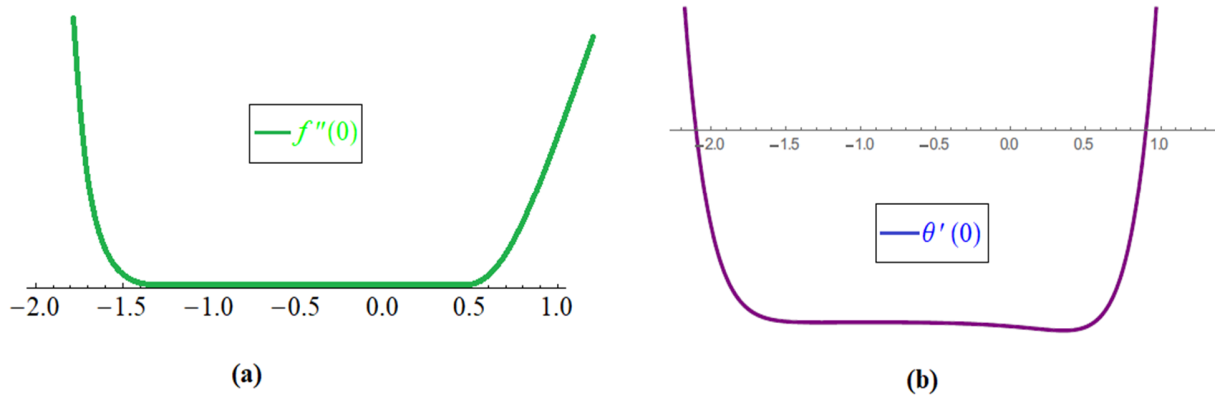
Figure 7: (a) $\hbar$-curve for velocity field (b) $\hbar$-curve for energy profile.

Table 3: The comparative analysis between the analytic and numerical techniques for $f'(1)$, $f''(1)$ & $\theta'(1)$.

Parameters		HAM			RK4			PCM		
Pr	**Bt**	$f'(0)$	$f''(0)$	$\theta'(0)$	$f'(0)$	$f''(0)$	$\theta'(0)$	$f'(0)$	$f''(0)$	$\theta'(0)$
6.0	0.3	2.43363	2.42378	0.258363	2.44965	2.42784	0.37006	2.43364	2.42379	0.258364
6.5	0.4	2.43776	2.42286	0.286760	2.43377	2.42092	0.40676	2.43778	2.42287	0.286762
6.5	0.5	2.36186	2.42193	0.315156	2.43790	2.42099	0.44342	2.36188	2.42194	0.315157
7.0	0.6	2.2508	2.24310	0.334805	2.24940	2.23612	0.53654	2.25090	2.24321	0.334813
7.5	0.6	2.07495	2.06278	0.351248	2.06953	2.05470	0.56303	2.07499	2.06289	0.351249

Table 4: The comparative analysis between the existing literature and present work for $f'(1)$, $f''(1)$ & $\theta'(1)$.

Parameters		Ref. [10]		HAM		RK4	
Pr	**Bt**	$f''(1)$	$\theta'(1)$	$f''(1)$	$\theta'(1)$	$f''(1)$	$\theta'(1)$
6.0	0.3	3.42371	0.358362	3.42378	0.358363	3.42784	0.47006
6.5	0.4	3.42283	0.386761	3.42286	0.386760	3.42092	0.50676
6.5	0.5	3.42192	0.415154	3.42193	0.415156	3.42099	0.54342
7.0	0.6	3.24314	0.434802	3.24310	0.434805	3.23612	0.63654
7.5	0.6	3.06275	0.451247	3.06278	0.451248	3.05470	0.66303

Table 5: The comparative analysis between the HAM and RK4.

	HAM				RK4			
ζ	$f(\zeta)$	$\theta(\zeta)$	$m(\zeta)$	$h(\zeta)$	$f(\zeta)$	$\theta(\zeta)$	$m(\zeta)$	$h(\zeta)$
0	0.5000	1.0000	1.0000	1.0000	0.5000	1.0000	1.0000	1.0000
1.0	0.5651	0.2930	0.4588	0.4436	0.5638	0.2916	0.4759	0.4577
2.0	0.6113	0.0914	0.1944	0.1842	0.6077	0.0869	0.2185	0.2042
3.0	0.6290	0.0312	0.0769	0.0722	0.6236	0.0270	0.0979	0.0903
4.0	0.6354	0.0112	0.0292	0.0273	0.6287	0.0088	0.0440	0.0397
5.0	0.6378	0.0040	0.0108	0.0101	0.6303	0.0030	0.0193	0.0173
6.0	0.6386	0.0015	0.0040	0.0037	0.6308	0.0011	0.0083	0.0074
7.0	0.6389	0.0005	0.0014	0.001	0.6310	0.0004	0.0035	0.0031
8.0	0.6391	0.0002	0.0005	0.0005	0.6311	0.0002	0.0014	0.0012
9.0	0.6391	0.00007	0.0002	0.0001	0.6312	0.0001	0.0004	0.0004
10.0	0.6391	0.00002	0.00007	0.0000	0.6312	0.0000	0.0000	0.0000

7.   Conclusion

We have studied, the incompressible, unsteady electro viscous fluid flow across two parallel plates with heat transmission. The phenomena have been formulated in form of the system of PDEs. Further, the modeled equations are simplified via a similarity framework to the system of ODEs. The HAM and RK4 techniques are implemented for the solution of the problem. Based on the above computation, the key findings are.

- The axial $f(\xi)$ and radial velocity of fluid reduces with the enhancement of Reynolds number R_1.
- The magnetic-based Reynold number R_3 improves both the radial and axial velocity $f'(\xi)$ of fluid flow.
- The magnetic strength profile $m'(\xi)$ can be reduced by the action of Bt, while it can be increased with the rising credit of velocity-based Reynold number R_2.
- Fluid temperature significantly declines with the increment of Prandtl number Pr and R_2.
- The numerical technique RK4 is a fast convergence method towards its solution than the analytic technique HAM.

Availability of data
Data are available in the article or supplementary material.

Competing interests
Authors declare that they have no competing interest.

References

[1] Turkyilmazoglu, M. (2010). The MHD boundary layer flow due to a rough rotating disk. *ZAMM-Journal of Applied Mathematics and Mechanics/Zeitschrift für Angewandte Mathematik und Mechanik: Applied Mathematics and Mechanics*, *90*(1), 72-82.

[2] M.J. Stefan, Versuch ber die scheinbare adhesion, Akademie der Wissenschaften, Mathematics che - Naturwissenschaftliche . 1874 69:713-721.

[3] M. Mahmood, S. Asghar, M.A. Hossain. Squeezed flow and heat transfer over a porous surface for viscous fluid. Heat Mass Transfer. (2007) 44: 165-173.

[4] M. Mustafa, T. Hayat, S. Obaidat. On heat and mass transfer in the unsteady squeezing flow between parallel plates. Meccanica. 2012 47:1581-1589.

[5] Hauck, M., Orlik, J., Levandovskyy, V., & Lykhachova, O. (2022). Symbolic homogenization and structure optimization for a periodically perforated cylindrical shell. *ZAMM-Journal of Applied Mathematics and Mechanics/Zeitschrift für Angewandte Mathematik und Mechanik*, *102*(1), e202100227.

[6] Bhatti, M. M., Phali, L., & Khalique, C. M. (2021). Heat transfer effects on electro-magnetohydrodynamic Carreau fluid flow between two micro-parallel plates with Darcy–Brinkman–Forchheimer medium. *Archive of Applied Mechanics*, *91*(4), 1683-1695.

[7] Ikram, M. D., Asjad, M. I., Akgül, A., & Baleanu, D. (2021). Effects of hybrid nanofluid on novel fractional model of heat transfer flow between two parallel plates. *Alexandria Engineering Journal*, *60*(4), 3593-3604.

[8] Gul, T., Bilal, M., Shuaib, M., Mukhtar, S., & Thounthong, P. (2020). Thin film flow of the water-based carbon nanotubes hybrid nanofluid under the magnetic effects. *Heat Transfer*, *49*(6), 3211-3227.

[9] Alhowaity, A., Bilal, M., Hamam, H., Alqarni, M. M., Mukdasai, K., & Ali, A. (2022). Non-Fourier energy transmission in power-law hybrid nanofluid flow over a moving sheet. *Scientific Reports*, *12*(1), 1-12.

[10] Bilal, M., Ahmed, A. E. S., El-Nabulsi, R. A., Ahammad, N. A., Alharbi, K. A. M., Elkotb, M. A., ... & SA, Z. A. (2022). Numerical Analysis of an Unsteady, Electroviscous, Ternary Hybrid Nanofluid Flow with Chemical Reaction and Activation Energy across Parallel Plates. *Micromachines*, *13*(6), 874.

[11] Algehyne, E. A., Alhusayni, Y. Y., Tassaddiq, A., Saeed, A., & Bilal, M. (2022). The study of nanofluid flow with motile microorganism and thermal slip condition across a vertical permeable surface. *Waves in Random and Complex Media*, 1-18.

[12] Alharbi, K. A. M., Ahmed, A. E. S., Ould Sidi, M., Ahammad, N. A., Mohamed, A., El-Shorbagy, M. A., ... & Marzouki, R. (2022). Computational Valuation of Darcy Ternary-Hybrid Nanofluid Flow across an Extending Cylinder with Induction Effects. *Micromachines*, *13*(4), 588.

[13] Alsallami, S. A., Zahir, H., Muhammad, T., Hayat, A. U., Khan, M. R., & Ali, A. (2022). Numerical simulation of Marangoni Maxwell nanofluid flow with Arrhenius activation energy and entropy anatomization over a rotating disk. *Waves in Random and Complex Media*, 1-19.

[14] Al-Mubaddel, F. S., Allehiany, F. M., Nofal, T. A., Alam, M. M., Ali, A., & Asamoah, J. K. K. (2022). Rheological Model for Generalized Energy and Mass Transfer through Hybrid Nanofluid Flow Comprised of Magnetized Cobalt Ferrite Nanoparticles. *Journal of Nanomaterials*, *2022*.

[15] Bilal, M., Gul, T., Alsubie, A., & Ali, I. (2021). Axisymmetric hybrid nanofluid flow with heat and mass transfer amongst the two gyrating plates. *ZAMM-Journal of Applied Mathematics and Mechanics/Zeitschrift für Angewandte Mathematik und Mechanik*, e202000146.

[16] Helmy KA. MHD unsteady free convection flow past a vertical porous plate. ZAMM Journal of Applied Mathematics and Mechanics/ZeitschriftfrAngewandteMathematik und Mechanik. Applied Mathematics and Mechanics. 1998 (4)78: 255-70.

[17] Ahmadian, A., Bilal, M., Khan, M. A., & Asjad, M. I. (2020). Numerical analysis of thermal conductive hybrid nanofluid flow over the surface of a wavy spinning disk. *Scientific reports*, *10*(1), 1-13.

[18] Rashidi MM, Ganesh NV, Hakeem AA, Ganga B. Buoyancy effect on MHD flow of nanofluid over a stretching sheet in the presence of thermal radiation. Journal of Molecular Liquids. 2014 (1)198: 234-8.

[19] Lv, Y. P., Algehyne, E. A., Alshehri, M. G., Alzahrani, E., Bilal, M., Khan, M. A., & Shuaib, M. (2021). Numerical approach towards gyrotactic microorganisms hybrid nanoliquid flow with the hall current and magnetic field over a spinning disk. *Scientific Reports*, *11*(1), 1-13.

[20] Tassaddiq, A., Khan, S., Bilal, M., Gul, T., Mukhtar, S., Shah, Z., & Bonyah, E. (2020). Heat and mass transfer together with hybrid nanofluid flow over a rotating disk. *AIP Advances*, *10*(5), 055317..

[21] Sharma, D., & Sood, S. (2022). Effect of inclined magnetic field on flow of Williamson nanofluid over an exponentially stretching surface in Darcy-Forchheimer model. *ZAMM-Journal of Applied Mathematics and Mechanics/Zeitschrift für Angewandte Mathematik und Mechanik*, e202100425.

[22] Shuaib, M., Shah, R. A., & Bilal, M. (2021). Von-Karman rotating flow in variable magnetic field with variable physical properties. *Advances in Mechanical Engineering*, *13*(2), 1687814021990463.

[23] Hayat T, Imtiaz M, Alsaedi A, Almezal S. On Cattaneo-Christov heat flux in MHD flow of Oldroyd-B fluid with homogeneous-heterogeneous reactions. Journal of Magnetism and Magnetic Materials. 2016 401: 296-303.

[24] Khashi'ie, N. S., Wahid, N. S., Arifin, N. M., & Pop, I. (2022). Magnetohydrodynamics unsteady separated stagnation-point (USSP) flow of a hybrid nanofluid on a moving plate. *ZAMM-Journal of Applied Mathematics and Mechanics/Zeitschrift für Angewandte Mathematik und Mechanik*, e202100410.

[25] Ali, A., Maqsood, M., Anjum, H. J., Awais, M., & Sulaiman, M. (2022). Analysis of heat transfer on MHD Jeffrey nanofluid flow over nonlinear elongating surface of variable thickness. *ZAMM-Journal of Applied Mathematics and Mechanics/Zeitschrift für Angewandte Mathematik und Mechanik*, *102*(2), e202100250.

[26] Bilal, M., Gul, T., Mouldi, A., Mukhtar, S., Alghamdi, W., Bouzgarrou, S. M., & Feroz, N. (2022). Melting Heat Transition in a Spinning Flow of Silver-Magnesium Oxide/Engine Oil Hybrid Nanofluid Using Parametric Estimation. *Journal of Nanomaterials*, *2022*.

[27] Alhowaity, A., Hamam, H., Bilal, M., & Ali, A. Numerical study of Williamson hybrid nanofluid flow with thermal characteristics past over an extending surface. *Heat Transfer.*

[28] Ullah, I., 2022. Heat transfer enhancement in Marangoni convection and nonlinear radiative flow of gasoline oil conveying Boehmite alumina and aluminum alloy nanoparticles. International Communications in Heat and Mass Transfer, 132, p.105920

[29] Gebhart, B., Mollendorf, J. Viscous dissipation in external natural convection flows. Journal of fluid Mechanics. 1969 (1)38:97-107.

[30] Sene, N. Stokes first problem for heated flat plate with Atangana-Baleanu fractional derivative. Chaos, Solitons and Fractals. 2018 117: 68-75.

[31] Elattar, S., Helmi, M. M., Elkotb, M. A., El-Shorbagy, M. A., Abdelrahman, A., Bilal, M., & Ali, A. (2022). Computational assessment of hybrid nanofluid flow with the influence of hall current and chemical reaction over a slender stretching surface. *Alexandria Engineering Journal*, *61*(12), 10319-10331.

[32] Hussain, F., Saleem, S., Nazeer, M., Al-Mubaddel, F. S., Ali, A., Saleem, A., & Saleem, M. (2022). Mathematical modeling and numerical solution of cross-flow of non-Newtonian fluid: Effects of viscous dissipation and slip boundary conditions. *ZAMM-Journal of Applied Mathematics and Mechanics/Zeitschrift für Angewandte Mathematik und Mechanik*, *102*(3), e202100130.

[33] Khan, M. R., & Mao, S. (2022). Numerical solution of magnetohydrodynamics radiative flow of Oldroyd-B nanofluid toward a porous stretched surface containing gyrotactic microorganisms. *ZAMM-Journal of Applied Mathematics and Mechanics/Zeitschrift für Angewandte Mathematik und Mechanik*, e202100388.

[34] S.J. Liao. The proposed homotopy analysis technique for the solution of nonlinear problems. PhD thesis. Shanghai Jiao Tong University. 1992.

[35] Liao S. Beyond perturbation: introduction to the homotopy analysis method. Chapman and Hall/CRC. 2003.

[36] Bilal, M., Khan, I., Gul, T., Tassaddiq, A., Alghamdi, W., Mukhtar, S., & Kumam, P. (2021). Darcy-Forchheimer Hybrid Nano Fluid Flow with Mixed Convection Past an Inclined Cylinder. *CMC-COMPUTERS MATERIALS & CONTINUA*, *66*(2), 2025-2039.

[37] Gul, T., Bilal, M., Alghamdi, W., Asjad, M. I., & Abdeljawad, T. (2021). Hybrid nanofluid flow within the conical gap between the cone and the surface of a rotating disk. *Scientific Reports*, *11*(1), 1-19.

[38] Gul, T., Rahman, J. U., Bilal, M., Saeed, A., Alghamdi, W., Mukhtar, S., ... & Bonyah, E. (2020). Viscous dissipated hybrid nanoliquid flow with Darcy–Forchheimer and forced convection over a moving thin needle. *AIP Advances*, *10*(10), 105308.

[39] Shah RA, Shuaib M, Ullah M, Khan A. Free Convection from an Infinite Disk Rotating in a Vertical Plane with Variable Magnetic Force. Journal of Computational and Theoretical Nanoscience. 2017 (9)14: 4340-51.

[40] Khan A, Shah RA. Influence of cross-diffusion and radiation on mixed convection between rotating discs in the presence of a variable magnetic field. The European Physical Journal Plus. 2019 (2)134: 52.